

Magneto-absorption spectra of Bernal graphite

Yen-Hung Ho,¹ Yu-Huang Chiu,² Wu-Pei Su,^{3,a)} and Ming-Fa Lin^{2,b)}

¹Department of Physics, National Sun Yat-Sen University, Kaohsiung 804, Taiwan

²Department of Physics, National Cheng Kung University, Tainan 701, Taiwan

³Department of Physics and Texas Center for Superconductivity, University of Houston, Houston, Texas 77204, USA

(Received 26 December 2010; accepted 16 June 2011; published online 8 July 2011)

With the availability of Landau wave functions in real space, we investigate the magneto-optical spectra of ordinary bulk graphite within a tight-binding model. The interlayer interactions significantly affect the structure, frequency and intensity of absorption peaks, as well as their field evolution and the double-peak absorptions. Those unique features of the absorption constitute important characterization of graphite and serve to differentiate the bulk spectra from those of true monolayer and bilayer graphenes. © 2011 American Institute of Physics. [doi:10.1063/1.3608383]

Graphene layers have in recent years attracted explosive attention for possible application to electronic devices.¹ The hexagonal crystal giving rise to exotic electronic properties is the main reason. In particular, the monolayer and coupled bilayer sheets are the simplest forms of few-layer systems; they respectively exhibit the massless and massive fermions.² Those band profiles in fact coexist in the ordinary bulk graphite.^{3,4} Therefore, a detailed inspection of bulk graphite is critical for a clear distinction between graphite and other graphene layers. Optical absorption spectrum is one of the most simple and straightforward way for subband characterization.^{3,4} Furthermore, a perpendicular magnetic field causes the planar electrons to undergo cyclotron motion, which effectively quantizes the spectral features so that they are more likely to be detectable and analyzable (Landau levels).^{5–9} In this Letter, the magneto-absorption spectra of bulk graphite are calculated and then compared to those of monolayer and bilayer.

The calculations of optical spectra are based on the Peierls tight-binding model which can be exactly diagonalized even with the inclusion of field-induced Peierls phases and all atomic interactions in the Hamiltonian.^{10–13} The calculated spectra are accurate for frequency range covering Landau-level transitions associated with π -electron orbitals (0–8 eV). More importantly, Landau-level wave functions in real space are also available. That permits numerical calculation of magneto-optical spectra and a clear characterization of the interaction between photons and electrons, including selection rules and absorption rates.^{11–13} In bulk graphite, the monolayer-like and bilayer-like absorption peaks are predicted to coexist with comparable intensity despite a large disparity in the density of states, whereas the electron-hole asymmetry is revealed as double-peak absorption lines. The calculated results provide a theoretical basis for future experiments to clarify the optical response of the graphene layers.^{7–9,14}

Bulk Bernal graphite consists of infinite graphene sheets with AB stacking sequence. At zero field, the primitive unit cell contains four atoms, the inequivalent A_l and B_l on respective layers $l=1,2$. The atomic couplings include γ'_0 between in-plane A - B atoms and γ'_i ($i=1-7$) between atoms

on different layers,^{2,15} as illustrated in Fig. 1(a). In the presence of a perpendicular magnetic field $B_0\hat{z}$, the Peierls phases are introduced in the wave functions, which enormously expand the periodic boundary conditions, the unit cell and the Hamiltonian.^{10,11,13} We utilize an exact diagonalization method which takes into account the field-induced Peierls phases and all atomic interactions simultaneously.^{10–13} In this way, both the Landau energy ($E^{c,v}$) and the wave functions in real space ($\psi^{c,v}$) are available. Moreover, they are accurate for all π electronic states.

The static magnetic field effectively quantizes the 3D electronic states into 1D Landau subbands, as shown in Fig. 1(c), where the corresponding range in reciprocal space is indicated in Fig. 1(b). The dispersive bands along planar momentum (blue and brown curves) are quantized into Landau levels, while the dispersions along k_z remain intact. The band edges mainly occur at the Brillouin zone boundaries, K and H points. Those at H are doubly degenerate compared to the

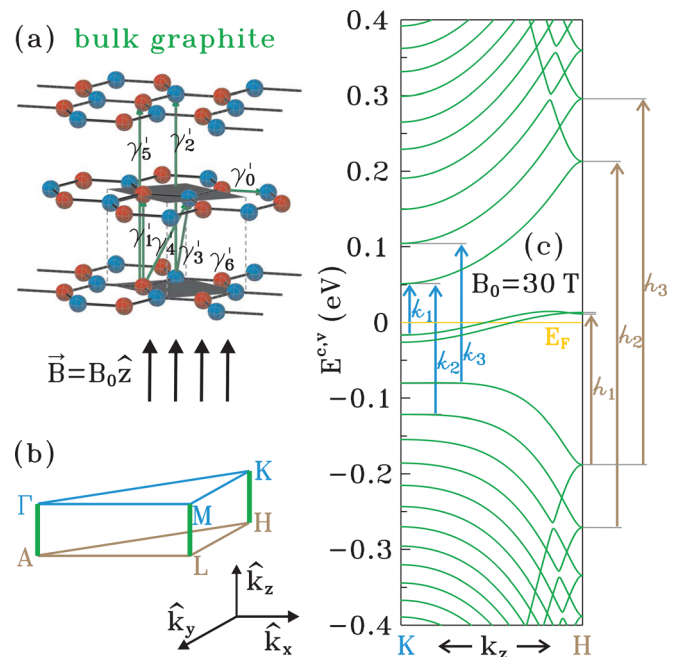


FIG. 1. (Color online) (a) Geometry of bulk graphite and (b) momentum space labeled with highly symmetric points. (c) k_z energy dispersions from K to H point at $B_0 = 30$ T.

^{a)}Electronic mail: wpsu@uh.edu.

^{b)}Electronic mail: mflin@mail.ncku.edu.tw.

K -point ones. The dispersion relations are dominated by the interlayer atomic hoppings $\gamma'_1 \sim \gamma'_7$. In particular, γ'_3 , γ'_4 , and γ'_6 are responsible for the electron-hole asymmetry. For the K -point band edges, the spacings between adjacent subbands in the valence states are narrower than those in the conduction states. However, such subband asymmetry is absent for the band edges at H . Moreover, the two kinds of band edges where charge carriers chiefly accumulate predominate the optical excitations.

With the absorption of a photon, electrons are excited from the occupied states to the unoccupied ones. The absorption spectra derived from the Fermi-Golden rule is given by¹⁶

$$A(\omega) \propto \int_{1stBZ} \frac{d\mathbf{k}}{(2\pi)^3} \left| \left\langle \psi^c \left| \frac{\hat{\mathbf{E}} \cdot \mathbf{P}}{m_e} \right| \psi^v \right\rangle \right|^2 \times \text{Im} \left\{ \frac{f(E^c) - f(E^v)}{E^c - E^v - \omega - i\Gamma} \right\}, \quad (1)$$

where $f(E^{c,v})$ is the Fermi-Dirac distribution. In our study, the incident light is linear-polarized with the plane of polarization parallel to the graphene sheet. The velocity matrix $\hat{\mathbf{E}} \cdot \mathbf{P}/m_e$ is evaluated in the gradient approximation, a suitable treatment for all carbon related systems.¹⁶ Within this approximation, the optical selection rules and the absorption rates can be determined in a fairly straightforward way.

The optical transitions between the 1D Landau subbands with parabolic dispersions result in the square-root divergences in the absorption spectra, as shown in Figs. 2(a)–2(c). Peak position corresponds to the energy difference between occupied and unoccupied states, mainly related to band edges at K and H points. The former are marked by blue dots and the latter by brown. Most of the K -point associated peaks occur in pairs, such as k_2 - k_3 . The small energy difference between the pair is due to electron-hole asymmetry. Those splittings decrease with increasing absorption energy or weakening field strength. As for the H -point transitions, the double-peaks are degenerate owing to the subband symmetry, e.g., h_2 - h_3 . Each of them is composed of two degenerate transitions and therefore appears as a “symmetric” square-root divergence. However, whether the transitions actually take place is subject to the characteristics of Landau wave functions which are described next.

All atomic sites in the extended unit cell can be classified into four sublattices, A_1 , A_2 , B_1 , and B_2 . From this viewpoint, the Landau wave functions in real space are well depicted by their probability distributions on the four sublattices, as shown in Fig. 3. Each of them behaves like a Hermite polynomial with the orders given by the relation $A_1:A_2:B_1:B_2 = n-1:n-1:n-2:n$. The velocity matrix elements are the first order derivatives of the Hamiltonian $\hat{\mathbf{E}} \cdot \mathbf{P}/m_e = \partial H/\partial k_{x,y}$; they are chiefly dominated by terms related to in-plane A - B hoppings (γ'_0) since γ'_0 is evidently stronger than $\gamma'_1 \sim \gamma'_7$. That is, the absorption rate is mainly determined by the product of the wave functions evaluated on the A and B atoms of the same layer, A_1 - B_1 and A_2 - B_2 . In addition, based on the orthogonality of Hermite polynomials, the product of two wave functions has a nonzero value only when they have the same oscillation number on the corresponding sublattices. The possible transitions between sublattices are indicated by the yellow dashed arrows. For K -point Landau states, their wave

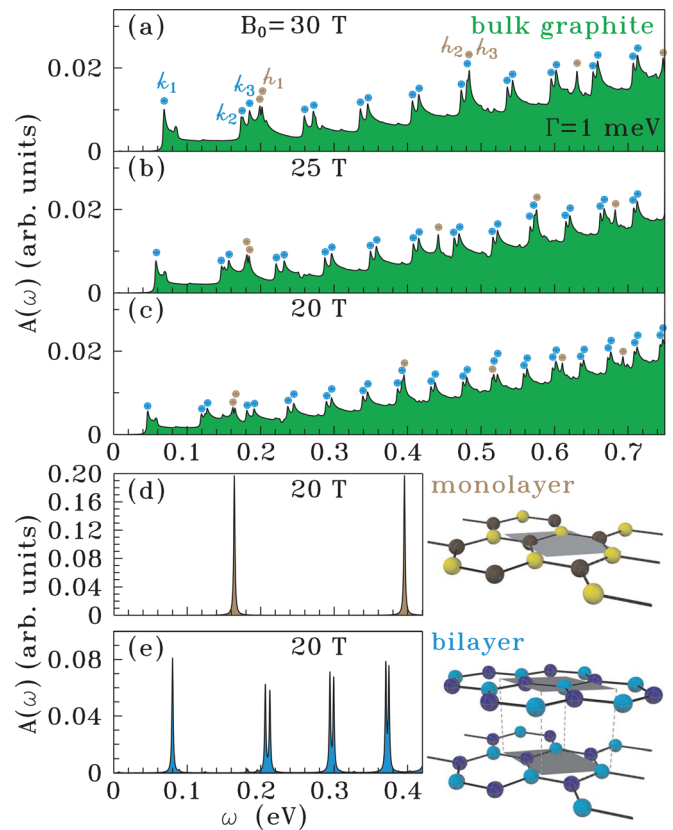


FIG. 2. (Color online) Magneto-absorption spectra of bulk graphite at (a) $B_0 = 30$ T, (b) 25 T, and (c) 20 T. The 20 T spectra of (d) monolayer and (e) bilayer graphene illustrated for comparison.

functions are composed of major $B_{1,2}$ and minor $A_{1,2}$ sublattices, resulting in the A_1 - B_1 and A_2 - B_2 transitions in each excitation channel (Fig. 3(a)). In contrast, the wave functions of H -point states are localized on A and B atoms of either layers, as shown in Fig. 3(b). Each absorption peak involves two excitation channels due to the degeneracy at the H point. Each

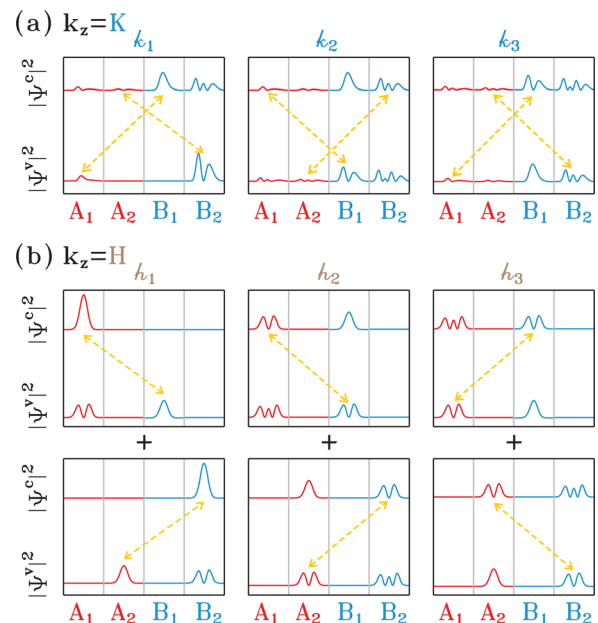


FIG. 3. (Color online) Probability distributions of valence and conduction Landau wave functions on the sublattices. Those related to transitions occurred at (a) K - and (b) H -point band edges.

channel possesses a single sublattice transition only; they are either A_1-B_1 or A_2-B_2 .

Two factors compete with each other in the peak intensity: the band-edge curvature with respect to k_z and the wavefunction characteristics. The subband curvatures at K -point edges are flatter than those at H . In this sense, the absorption peaks related to K point should predominate over the H -point ones. However, it turns out that the two kinds of peaks are actually almost equal in intensity. This unusual result can be explained by the way the wave function localizes on constituent sublattices. The optical transition rate is in direct proportion to the product of weights on same-layered A and B sublattices; they are weak-strong combinations at K point but strong-strong ones at H . That is why the H -point spectral intensity is comparable with K -point one. Therefore, in optical measurements, both types of signatures should be comparable in intensity.⁷⁻⁹ On the other hand, the density of states involves band curvatures only, hence, its H -point feature is about three times weaker than the K -point one (not shown).

The magneto-optical spectra of 2D monolayer and bilayer graphene are presented in Figs. 2(d) and 2(e) for comparison with that of 3D bulk graphite. The absorption peaks of 2D systems are delta-function-like, instead of square-root ones in 3D graphite. This is because the Landau levels developed from 2D band structures are dispersionless, in contrast to the 1D Landau subbands retained in 3D bulk. Moreover, the spectral structures in bulk graphite are much broader than in monolayer and bilayer, as seen by comparing Figs. 2(c)–2(e). This is due to the weaker Landau quantization in bulk graphite, which also leads to the overall weaker spectral intensity, as clearly seen in the vertical scale of Figs. 2(a)–2(e).

The optical transitions at K and H points have quite distinct field evolutions. The former type is close to a linear dependence whereas the latter is square-root like, as depicted by the blue and brown dots in Fig. 4(a). Compared with monolayer and bilayer systems, the absorption frequencies related to H point are fully identical to the monolayers (brown dots in Fig. 4(b)).⁵ However, those of K point are evidently reduced and the splitting in double peaks is significantly enhanced, compared to the bilayers (blue dots in Fig. 4(b)).⁶ This can be utilized to distinguish the true bilayer from the multilayered samples, as addressed in previous optical measurements.⁷⁻⁹ Whether the double peaks actually appear is also sensitive to the ambient temperature. For instance, they should be observable at temperature below 75 K for bilayers and 150 K for bulk graphite at $B_0 = 30$ T.

The numerical method we have developed can be generalized to other layered systems or other stacking sequences.¹² The determination of Landau wave functions enables one to further study many other interesting physical properties, such as transport, reflectance, and electronic Coulomb excitations.^{17,18}

To summarize, in the framework of a tight-binding model, the Landau wave functions are available through exact diagonalization of the Hamiltonian and can be used to explicitly resolve the magneto-optical spectra of bulk graphite. Both the monolayer-like and bilayer-like signatures are found to coexist in the bulk spectra. The optical selection rules and relative absorption rates intimately reflect impor-

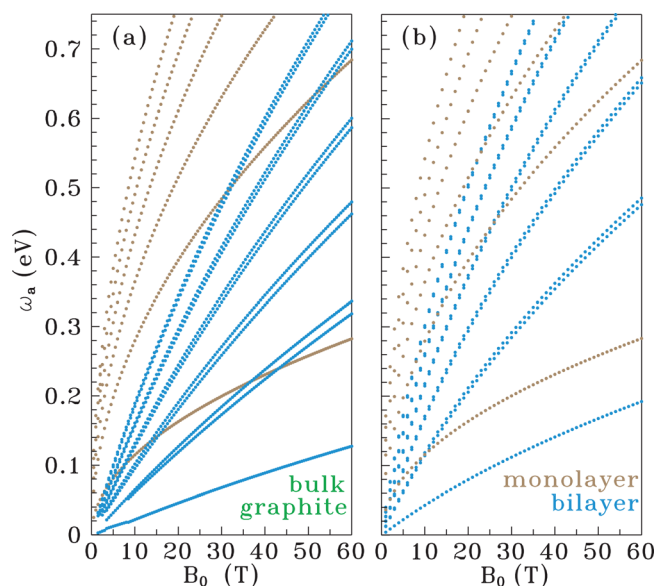


FIG. 4. (Color online) Field evolution of absorption lines in (a) bulk graphite, (b) monolayer and bilayer graphenes.

tant characteristics of the wave functions. Close inspection of absorption lines further reveals the spectral difference between graphite bulk and bilayer.

This work was supported by the NSC and NCTS of Taiwan, under Grant Nos. NSC 98-2112-M-006-013-MY4 and NSC 97-2112-M-110-009. W.P.S. was partially supported by the Texas Center for Superconductivity and the Robert A. Welch Foundation under Grant No. E-1070.

- ¹D. S. L. Abergel, V. Apalkov, J. Berashevich, K. Ziegler, and T. Chakraborty, *Adv. Phys.* **59**, 261 (2010).
- ²B. Partoens and M. F. Peeters, *Phys. Rev. B* **74**, 085406 (2006).
- ³S. Y. Zhou, G.-H. Gweon, J. Graf, A. V. Fedorov, C. D. Spataru, R. D. Diehl, Y. Kopelevich, D.-H. Lee, S. G. Louie, and A. Lanzara, *Nat. Phys.* **2**, 595 (2006).
- ⁴A. Gruneis, C. Attaccalite, T. Pichler, V. Zabolotnyy, H. Shiozawa, S. L. Molodtsov, D. Inosov, A. Koitzsch, M. Knupfer, J. Schiessling, R. Follath, R. Weber, P. Rudolf, L. Wirtz, and A. Rubio, *Phys. Rev. Lett.* **100**, 037601 (2008).
- ⁵R. S. Deacon, K.-C. Chuang, R. J. Nicholas, K. S. Novoselov, and A. K. Geim, *Phys. Rev. B* **76**, 081406(R) (2007).
- ⁶E. A. Henriksen, Z. Jiang, L.-C. Tung, M. E. Schwartz, M. Takita, Y.-J. Wang, P. Kim, and H. L. Stormer, *Phys. Rev. Lett.* **100**, 087403 (2008).
- ⁷M. Orlita, C. Faugeras, G. Martinez, D. K. Maude, M. L. Sadowski, and M. Potemski, *Phys. Rev. Lett.* **100**, 136403 (2008).
- ⁸M. Orlita, C. Faugeras, J. M. Schneider, G. Martinez, D. K. Maude, and M. Potemski, *Phys. Rev. Lett.* **102**, 166401 (2009).
- ⁹K.-C. Chuang, A. M. R. Baker, and R. J. Nicholas, *Phys. Rev. B* **80**, 161410(R) (2009).
- ¹⁰Y. H. Lai, J. H. Ho, C. P. Chang, and M. F. Lin, *Phys. Rev. B* **77**, 085426 (2008).
- ¹¹Y. H. Ho, Y. H. Chiu, D. H. Lin, C. P. Chang, and M. F. Lin, *ACS Nano* **4**, 1465 (2010).
- ¹²Y. H. Ho, J. Y. Wu, R. B. Chen, Y. H. Chiu, and M. F. Lin, *Appl. Phys. Lett.* **97**, 101905 (2010).
- ¹³Y. H. Ho, J. Y. Wu, Y. H. Chiu, J. Wang, and M. F. Lin, *Philos. Trans. R. Soc. A* **368**, 5445 (2010).
- ¹⁴Z. Q. Li, S.-W. Tsai, W. J. Padilla, S. V. Dordevic, K. S. Burch, Y. J. Wang, and D. N. Basov, *Phys. Rev. B* **74**, 195404 (2006).
- ¹⁵J. Nakao, *J. Phys. Soc. Jpn.* **40**, 761 (1976).
- ¹⁶M. F. Lin and K. W.-K. Shung, *Phys. Rev. B* **50**, 17744 (1994).
- ¹⁷J. H. Ho, C. L. Lu, C. C. Hwang, C. P. Chang, and M. F. Lin, *Phys. Rev. B* **74**, 085406 (2006).
- ¹⁸O. L. Berman, G. Gumbs, and Y. E. Lozovik, *Phys. Rev. B* **78**, 085401 (2008).